Northumbria Research Link

www.northumbria.ac.uk/nrl

northumbria
UNIVERSITY NEWCASTLE

Explicit simulation of bolted endplate composite beam-to-CFST column connections

Huu-Tai Thai [a,b,c,*], Thuc P. Vo [d,e,*], Trung-Kien Nguyen [f], Cao Hung Pham [g]

[a] Division of Construction Computation, Institute for Computational Science, Ton Duc Thang University, Ho Chi Minh City, Vietnam

[b] Faculty of Civil Engineering, Ton Duc Thang University, Ho Chi Minh City, Vietnam

[c] School of Engineering and Mathematical Sciences, La Trobe University, Bundoora, VIC 3086, Australia

[d] Duy Tan University, Da Nang, Vietnam

[e] Department of Mechanical and Construction Engineering, Northumbria University, Ellison Place, Newcastle upon Tyne NE1 8ST, UK

[f] Faculty of Civil Engineering, Ho Chi Minh City University of Technology and Education, 1 Vo Van Ngan Street, Thu Duc District, Ho Chi Minh City, Vietnam.

[g] School of Civil Engineering, The University of Sydney, Sydney, NSW 2006, Australia

Abstract

This paper explores the use of an explicit solver available in ABAQUS/Explicit to simulate the behaviour of blind bolted endplate connections between composite beams and concrete-filled steel tubular (CFST) columns. Main aspects of the explicit analysis such as solution technique, blind bolt modelling, choice of element type and contact modelling are discussed and illustrated through the simulation of a large-scale test on the considered joint. The mass scaling option and smooth step amplitude are very effective tools to speed up the explicit simulation. Shell elements can be used in modelling the I-beam due to their computational efficiency and accuracy in capturing local buckling effects. With a proper control of the loading rate, the explicit analysis can provide accurate and efficient predictions of the quasi-static behaviour of the bolted endplate composite connections.

Keywords: Bolted endplate connection; Concrete-filled steel tube; Blind bolt modelling; Explicit analysis

* Corresponding author.
E-mail address: tai.thai@latrobe.edu.au (H.T. Thai), thuc.vo@northumbria.ac.uk (T.P. Vo).

1. Introduction

Concrete-filled steel tubular (CFST) columns have been increasingly used in high-rise buildings in recent years. In order to connect a CFST column to steel or composite beams in these framed buildings, blind bolted endplate connections are favourably used in construction practice because of their economy and simplicity in the fabrication and assembly. Experimental results carried out by France et al. [1-3] indicated that the use of CFST columns provides a significant enhancement of both moment resistance and initial stiffness of blind bolted endplate connections as compared with that of tubular columns. A typical bolted endplate beam-to-CFST column connection shown in Fig. 1 is composed of the endplates welded to the end of the steel beams. This assembly is then connected to a CFST column using blind bolts or one-sided bolts.

Experimental studies have been carried out to predict the moment-rotation behaviour of bolted endplate beam-to-CFST column joints with steel beams [4-15] and composite beams [16-25]. However, as summarised in Thai and Uy [26], the number of tests on the considered joints is still limited due to expensive cost and time consuming. Therefore, finite element (FE) simulation becomes a cost-effective tool to predict moment-rotation behaviour of such connections. Several FE simulations of the bolted endplate beam-to-CFST column connections have been reported in the literature for considered joints with steel beams [10, 27-29]. Compared with steel connections, the modelling of composite connections is significantly more challenging since it involves in the complex contact interactions of additional components including concrete slab, profiled sheeting, shear connector and reinforcing bar. Kataoka and El Debs [30-31] developed a three-dimensional (3D) model for parametric study of composite connections under cyclic loadings using Diana software. Ataei et al. [32] developed a FE model of composite

joints using ABAQUS to calibrate with their proposed moment-rotation model. All joint components were modelled using brick elements (C3D8R) except the reinforcing bars using truss elements (T3D2). The Hollo-bolt was modelled as a standard bolt, and its contact interactions with endplates and CFST column were simply modelled by TIE constraints. However, their model cannot fully capture the local buckling of the beam flange due to using one layer of solid elements through the thickness [33]. In addition, due to the inappropriate modelling of the Hollo-bolt and its contact interactions, the initial stiffness of joints was not accurately predicted. These limitations were overcome in the work by Thai and Uy [33] by replacing brick elements (C3D8R) by shell elements (S4R) in the steel beam, and modelling accurately the Hollo-bolt's geometry and its contact interactions with endplates and CFST column. Recently, Ataei et al. [34-36] developed model for predicting moment-rotation relationship of demountable bolted endplate composite beam-to-column connections.

The development of an accurate and reliable FE model to predict the behaviour of connections is still very limited due to the difficulty in the modelling of such large deformation and complex contact problems. Compared with the implicit analysis, the explicit method is more suitable for simulating the considered connections since it is avoidable numerical convergence difficulties encountered in the implicit solver due to large deformation and multiple contact interactions between joint components. Although explicit modelling of connections has been reported by Thai and Uy [33], the main issues involving the explicit analysis for such connections has not been presented. Therefore, this main objective of this paper is to discuss the issues related with the FE simulation of connections using the explicit solver available in ABAQUS/Explicit. A large-scale test on the studied connection is used for illustrative purposes.

2. Simulation of a large-scale test on the considered joint

2.1. Description of the tested specimen

A large-scale test (specimen CJ1) on the considered connection conducted by Loh et al. [16] was selected to serve as a reference to discuss the aspects of the explicit analysis of connections. The configuration details of the tested specimen are shown in Fig. 2. The joint consists of two steel beams of 250UB25.7 connected to a square hollow section (SHS) column of SHS 200×9 to form the cruciform arrangement which simulates the internal region of a composite frame. A 12 mm thick flush endplate was welled to the end of the steel beam by 8 mm thick fillet welds. This assembly was then connected to the column using eight M20 Hollo-bolts. A 120 mm deep concrete slab was supported by the Bondek profiled sheeting which was placed longitudinally with welded-through headed stud shear connectors of $\phi19\times100$ mm. The main reinforcement of $4\phi16$ was distributed in one layer with equal spacing over the width of the slab. The length of the specimens can accommodate five shear connectors to be placed on each cantilever beam to provide full composite action with the steel beam.

Material properties of structural steels were given in Table 1. The compressive and tensile strengths of concrete are 17.5 MPa and 1.7 MPa, respectively. The specimen was put upside down, and a loading rate of 0.4mm/min in the linear elastic range was applied to the CFST column and then increased to 1.0 mm/min in the nonlinear range towards the failure [16].

2.2. FE modelling

The computational time can be reduced if only a half of the specimen was modelled as shown in Fig. 3 due to the inherent symmetry of the problem. The FE mesh of the

4

half of the specimen was illustrated in Fig. 4. Details of the element type and mesh sizes of individual components were determined by Thai and Uy [33] based on mesh convergence studies. In addition to the contact simulation which will be discussed in the next section, the constraint conditions were also applied to joint components. For example, the *tie* constraint was used to tie the profiled sheeting to the bottom surface of concrete slab, whilst the steel beam was tied to the endplate using *shell-to-solid coupling* constraint because they were modelled by two different element types. The *embedded region* constraint was used to embed the reinforcement and shear connector into concrete slab. The *rigid body* constraint was used to tie the end cross-section of the CFST column to a reference point located at the centre of the cross-section (see Fig. 3). Vertical load was applied through the reference point via a displacement control method. Material models used in ABAQUS for modelling structural steel and concrete materials have been calibrated by Thai and Uy [33]. All simulations illustrated in this study were performed using a desktop computer with 3.6 GHz Core i7 with 32 GB RAM configuration.

3. Modelling aspects

3.1. Explicit solution technique in ABAQUS/Explicit

In ABAQUS, there are two different types of solution strategies: the implicit method available in ABAQUS/Standard and the explicit method available in ABAQUS/Explicit. The implicit solution of a nonlinear problem at each increment is obtained based on an iteration process to enforce equilibrium conditions. Since the implicit method requires an inversion of stiffness matrix, it is too computationally expensive for large problems. For complex contact problems as seen in the considered joint, the implicit method

usually encounters severe convergence difficulties since a large number of iterations are needed to satisfy contact conditions. In contrast, the explicit solution of a nonlinear problem at the current state is obtained based on the kinematic state from the previous increment, and thus the inversion of the stiffness matrix is not necessary. In addition, no iterations are required in the explicit method to enforce contact conditions. As a result, the severe convergence difficulties encountered in the implicit method for complicated contact problems can be overcome in the explicit analysis.

3.1.1. Speeding up the simulation

Running time in the explicit analysis is a function of not only the model size, but also the time increment size. In the explicit solver, the time increment is internally calculated to satisfy the stability limit Δt which is a function of element size L, Young's modulus E and density ρ of materials ($\Delta t = L\sqrt{\rho / E}$). Since the stability limit is usually very small, it is computationally impractical if the quasi-static loading rate is used in the simulation because of requiring a large number of increments to complete the simulation. Therefore, in order to obtain an economical quasi-static solution, the simulation needs to be sped up by using the *smooth step* amplitude and increasing the time increment size.

To illustrate the effect of using the *smooth step* amplitude, Fig. 5 compared the load-displacement curves predicted by the FE simulations using the *smooth step* and linear step (*tabular*) amplitudes with the experimental result tested by Loh et al. [16]. These amplitudes shown in Fig. 6 were applied to the displacement control at the end cross-section of the column with a loading rate of 6.25 mm/min which is 15 times greater than the loading rate used in the test. It can be observed that if the smooth step was used, the predicted response was very smooth and close to the test result [16]. Meanwhile, the

response generated by the linear step exhibited some vibrations due to inertial dynamic effects, especially in the initial range when the behaviour of the connection is linear elastic.

Another alternative to speed up the explicit simulation is to increase the time step size, i.e. the stability limit $\Delta t = L\sqrt{\rho/E}$, through increasing the element size and density or reducing Young's modulus. While increasing the element size is usually impractical for structures with complex geometries, reducing Young's modulus will affect accuracy due to the change in the stiffness of the model. Therefore, the only way to increase the time step is to increase density of the smallest elements which control the time step through the *mass scaling* option. Mass scaling is suitable for quasi-static problems where the velocity is low and the kinetic energy is very small compared to the internal energy. In this method, mass should be added to non-critical regions of the model. To demonstrate the effects of the mass scaling method, Fig. 7 showed the comparison of the explicit solutions with and without using mass scaling. The corresponding CPU times were also given. The mass scaling was applied to the smallest elements at the bolt shank which control the time step. The time step Δt was increased from 3.05×10^{-5} s (without mass scaling) to 5.38×10^{-5} s when the mass of the bolt shank was scaled up four times. It can be seen from Fig. 7 that the explicit solutions of two cases are almost identical. In other words, the additional mass assigned to the bolt shank has negligible effect on the response of the joint, but it can reduce the CPU time up to 42 %.

3.1.2. Time period used in the simulation

It is noted that the response generated by the explicit method is transient and strongly dependent on the loading rate used. Therefore, it is computationally expensive for quasi-

7

static problems if the quasi-static loading rate is modelled exactly since a large number of increments are needed to complete the simulation. In order to obtain an economical solution, i.e. a sufficiently accurate prediction in the shortest time period, the simulation time was usually scaled down to a time period in which the inertial dynamic effects become significant. Based on the classical dynamic theory, the transient response of a dynamic system can be approximately treated as quasi-static one if the loading duration is large compared to the natural period of the system [37]. For complex structures, however, this statement does not give any direct guidance on the exact time period needed in the simulation. Therefore, a trial and error process is usually used to determine the maximum viable loading period.

Fig. 8 showed the load-displacement responses of the connection at three loading rates of 25, 12.5 and 6.25 mm/min, corresponding to the time periods of 0.05, 0.1 and 0.2 s. It can be seen that the response of the joint under the loading rate of 25 mm/min exhibited vibration due to inertial dynamic effects. It also overestimated the initial stiffness and resistance of the connection. If the loading time was reduced, the predicted response would become smoother. Since the loading rate of 6.25 mm/min provides the prediction close to the test result [16], it can be considered as the maximum viable loading rate that can be used to simulate the quasi-static response of the studied connection. It should be noted that the actual loading rate used in the experiment is only 0.4mm/min [16] which is 15 times smaller than the one used in the simulation.

3.1.3. Validating the explicit solution

If the experimental result was not available, the accuracy of explicit solutions can be verified by checking the energy output. Based on ABAQUS/Explicit manual [38], the explicit solution can be considered as a quasi-static one if the ratio of the kinetic energy

(KE) to the internal energy (IE) is less than 10 %. Fig. 9 compared the KE and IE outputs of the whole model at different loading rates. Although the IEs are almost similar at different loading rates, the KEs reduce significantly when the loading rate decreases. As a result, decreasing the loading rate will lead to a reduction in the KE-to-IE ratio as illustrated in Fig. 10. Based on the energy criterion stated in ABAQUS, only the explicit solution at the loading rate of 6.25 mm/min can be considered as quasi-static solution since its KE-to-IE ratio is less than 10 %.

Another method to validate the explicit solution is to check the equilibrium of the applied load and the reaction force. The explicit solution can be considered as a quasi-static one if the obtained reaction is approximately equal to the applied load. Fig. 11 showed the comparison between the applied load and the reaction force of a half of the connection at different loading rates. In order to obtain the applied load, the load control method was used in the explicit simulation. It can be seen that the reaction force of the joint under the loading rate of 25 mm/min exhibited some differences with the applied load. These differences become smaller when the loading rate decreases. At the loading rate of 6.25 mm/min, the obtained reaction force is almost identical with the applied load (see Fig. 11c), and thus the explicit solution at this loading rate can be considered as quasi-static solution.

3.2. Modelling of Hollo-bolt

One-sided bolts or blind bolts are designed to be installed from one side or the outer side of the tube. There are several types of commercially available blind bolts such as Hollo-bolt, Ajax Oneside bolt, Huck bolt and Flowdrill system. Unlike other blind bolts, the geometries of Hollo-bolt's before and after tightening are totally different as shown in Fig. 12. This difference enhances both initial stiffness and moment resistance of the

9

joint if the tubular column is filled in with concrete. Therefore, to obtain an accurate prediction, the Hollo-bolt's geometry should be carefully modelled. In this study, a simplified bolt model proposed by Thai and Uy [33] in Fig. 12c was adopted to illustrate the Hollo-bolt modelling. The pretension in the Hollo-bolt was included in the explicit analysis by means of an initial temperature assigned to the bolt shank (see Fig. 12c) because the bolt load tool is not available in ABAQUS/Explicit. More details of this approach can be found in Thai and Uy [33]. In the test conducted by Loh et al. [16], the Hollo-bolt was tightened up to 300 Nm torque corresponding to an initial tension of 76 kN or an initial stress of 310 MPa.

In the explicit method, the mesh size is very sensitive to the computational cost of the simulation since it involves not only in the number of degree of freedom (DOF) but also in the calculation of time increment size. To investigate the effect of mesh size on the structural response and computational time, three different mesh sizes shown in Fig. 13 were used in the modelling of Hollo-bolt. Each mesh was notated by two numbers in which the first number indicates the number of elements around the perimeter of the bolt, whilst the second number indicates the number of elements along the radius of the bolt shank. The meshes of the endplate, infilled concrete and column hole are also changed according to the mesh of the Hollo-bolt so that contact interaction between them can share the same mesh. Fig. 14 showed the distribution of the von Mises stresses of the Hollo-bolt due to the pretension. As expected, the von Mises stresses distributed in the Hollo-bolt become more uniform if a finer mesh is used. There is a stress concentration observed in the case of the coarse mesh (Mesh 1). Fig. 15 showed a comparison of the load-displacement responses of the connection predicted by three different meshes with the experimental results [16]. The CPU times of three simulations

were also provided in Table 2. It can be seen that the responses generated by three meshes are very close each other until the post-buckling phase. In other words, the initial stiffness, ultimate resistance and pre-buckling response of the connection are not sensitive to the mesh size of the bolt. This is due to the fact that the global behaviour of bolted endplate connections was not controlled by the bolt. By comparing with the experimental result, Mesh 2 would be the optimum choice when considering both the accuracy and computational efficiency.

3.3. Selection of element type

In the considered connection, the reinforcement, profiled sheeting and concrete are obviously modelled by beam, shell and solid elements, respectively, due to their naturally 1D, 2D and 3D behaviour. However, the steel tube, endplate and steel beam can be modelled by either solid or shell elements. Compared with the solid element, the shell element is not only more computationally efficient due to involving less number of DOF, but also provides a better prediction of the behaviour of the connection (see Fig. 16) and local buckling effects (see Fig. 17). However, for contact problems which require accurate representation of the geometry, the use of solid elements is unavoidable since shell elements cannot sufficiently represent their physical thickness. Based on these facts, the profiled sheeting and steel beams will be modelled by shell elements (S4R), whilst the remaining components of the joint except for the reinforcement will be modelled by brick elements (C3D8R).

3.4. Contact modelling

In addition to the constraint conditions, the interactions between contacting surfaces of the joint components also need to be modelled using either the *general contact* or

11

surface-to-surface contact types available in ABAQUS/Explicit. In the *general contact* type, many contact pairs can be defined at the same time, and the contact region is not necessary to be continuous as in the case of the *surface-to-surface contact* type. The *general contact* is therefore adopted in this study. In this contact algorithm, a finite-sliding formulation with a penalty method was used to enforce contact constraints between the contact pairs. This formulation allows for arbitrary separation, sliding and rotation of the surfaces in contact. The penalty method enforces both the normal contact behaviour with a "hard" pressure-overclosure relationship and the tangential behaviour with Coulomb friction model. This method is computationally efficient for modelling friction. Only the penalty enforcement-based finite-sliding formulation is currently available for the *general contact* type in ABAQUS/Explicit.

In this connection, eight contact pairs were used in the *general contact* type to define the interaction of the components in the joint. Details of each contact pair can be found in [33]. It is also noted that for each contact pair the selection of master or slave surfaces is not necessary [39]. In addition, in order to reduce the analysis time, the mesh between contacting surfaces in each contact pair should be the same. The contacting surfaces around the bolt and contact pressure in the bolt due to the bolt pretension were illustrated in Fig. 18.

4. FE analysis

In this section, the behaviour of all components of the considered connection during the loading progress was examined through the FE analysis. The global behaviour of the connection is characterised by the load-deflection curve shown in Fig. 19. The specific values of the applied load and corresponding displacement at critical points were also summarized in Table 3. The distribution of von Mises stresses in all components at the

ultimate load was shown in Fig. 20.

It can be seen from Fig. 19 that the first critical point due to the initial crack occurred in the concrete slab was detected at very low loading level (around 6% of the ultimate load). The distribution of the tensile damage parameter in the concrete slab shown in Fig. 21 indicated that the crack first initiated at the top surface of the corner of the column and slab, and propagated towards the slab edge and the bottom surface when the loading increased. The relationship between the applied load and the crack width at the top surface of the concrete slab was illustrated in Fig. 22. There is a slight change in the slope of the load-crack width curve after the formation of the first crack concrete slab at a loading level of 21 kN. When the applied load is greater than 280 kN, the slope of the load-crack width curve reduces significantly due to remarkably widening of the crack. This in turn leads to a considerable reduction in the slope of the load-deflection curve (see Fig. 19).

Fig. 19 also indicated that after the formation of the first crack in concrete slab, the joint stiffness remains almost unchanged until the first yielding appears at the bottom flange of the steel beam (critical point 2) and the headed stud (critical point 3). By further increasing the applied load, the joint stiffness reduces slightly till the first yielding detected in the endplate (critical point 4) and the steel column (critical point 5). After the yielding in the reinforcement is formed (critical point 6), the reduction in stiffness becomes significant as the loading increased further. The explanation for this fact might be due to the loss of the bond between the reinforcing bar and surrounding concrete caused by progressively widening of the crack as shown in Fig. 22.

As shown in Fig. 20b-d, the stresses in the steel column, endplate and steel beam were concentrated at the interaction region between the endplate, the bottom flange and

13

lower part of the web. This is expected because of the transfer of the compression force in the compression zone of the composite beam under hogging moment. Due to the confining effects of the steel tubular column, the maximum von Mises stress found in the infilled concrete is up to 53.6 MPa (see Fig. 20a) which is three times greater than the compressive strength of concrete. Similar observation was also found in the concrete slab in Fig. 20a. Therefore, these effects should be included in the modelling of concrete material. It is observed from Fig. 20e that the stress in the headed stud shear connector was concentrated in the region welded to the beam flange. This is expected since the longitudinal shear force in the concrete slab will transfer to the steel beam through this welded region. The Hollo-bolt in the considered connection was not yielded since the maximum von Mises stress concentrated at the interaction with the endplate and column is much smaller than its yield stress (see Fig. 20f). It is observed from Fig. 20g,h that the stresses in the profiled sheeting and reinforcement were concentrated at the region around the connection.

5. Conclusions

This paper presents an explicit approach to analyse blind bolted endplate beam-to-CFST column connections. Several issues concerned with the explicit analysis are addressed and illustrated through the modelling of a large-scale test. The following points can be outlined from the present study:

(1) The *mass scaling* option and *smooth step* amplitude are very effective tools to speed up the explicit simulation. These useful tools make the explicit method attractive and applicable to simulate the quasi-static behaviour of bolted endplate connections.

(2) The explicit analysis can provide accurate and efficient predictions of the quasi-static responses of the studied connection if the loading rate is properly controlled.

(3) To obtain an accurate prediction of the initial stiffness of the joint, special attention should be paid to the modelling of the geometry of the Hollo-bolt. The mesh size of the Hollo-bolt only affect the stress distribution in and around the bolt, but it is not sensitive to the global response of connections.

(4) Unless an accurate representation of the geometry of shell structures is required, shell elements should be used in modelling due to their computational efficiency and accuracy in capturing local buckling effects. This statement is correct for both thin and thick shell structures since the S4R shell element provided in ABAQUS is applicable for the analysis of both thin and thick shells.

Acknowledgements

References

[1]   France JE, Buick Davison J, A. Kirby P. Strength and rotational response of moment connections to tubular columns using flowdrill connectors. Journal of Constructional Steel Research 1999;50:1-14.

[2]   France JE, Buick Davison J, A. Kirby P. Moment-capacity and rotational stiffness of endplate connections to concrete-filled tubular columns with flowdrilled connectors. Journal of Constructional Steel Research 1999;50:35-48.

[3]   France JE, Buick Davison J, Kirby PA. Strength and rotational stiffness of simple connections to tubular columns using flowdrill connectors. Journal of Constructional Steel Research 1999;50:15-34.

[4]   Wang JF, Han LH, Uy B. Behaviour of flush end plate joints to concrete-filled

steel tubular columns. Journal of Constructional Steel Research 2009;65:925-939.

[5]   Wang JF, Han LH, Uy B. Hysteretic behaviour of flush end plate joints to concrete-filled steel tubular columns. Journal of Constructional Steel Research 2009;65:1644-1663.

[6]   Wang JF, Guo S. Structural performance of blind bolted end plate joints to concrete-filled thin-walled steel tubular columns. Thin-Walled Structures 2012;60:54-68.

[7]   Wang JF, Chen L. Experimental investigation of extended end plate joints to concrete-filled steel tubular columns. Journal of Constructional Steel Research 2012;79:56-70.

[8]   Wang JF, Chen X, Shen J. Performance of CFTST column to steel beam joints with blind bolts under cyclic loading. Thin-Walled Structures 2012;60:69-84.

[9]   Wang JF, Zhang L, Spencer Jr BF. Seismic response of extended end plate joints to concrete-filled steel tubular columns. Engineering Structures 2013;49:876-892.

[10] Tizani W, Al-Mughairi A, Owen JS, Pitrakkos T. Rotational stiffness of a blind-bolted connection to concrete-filled tubes using modified Hollo-bolt. Journal of Constructional Steel Research 2013;80:317-331.

[11] Tizani W, Wang ZY, Hajirasouliha I. Hysteretic performance of a new blind bolted connection to concrete filled columns under cyclic loading: An experimental investigation. Engineering structures 2013;46:535-546.

[12] Tizani W, Pitrakkos T. Performance of T-stub to CFT joints using blind bolts with headed anchors. Journal of Structural Engineering 2015;141:04015001.

[13] Pitrakkos T, Tizani W. A component method model for blind-bolts with headed anchors in tension. Steel and Composite Structures 2015;18:1305-1330.

[14] Wang ZB, Tao Z, Li DS, Han LH. Cyclic behaviour of novel blind bolted joints with different stiffening elements. Thin-Walled Structures 2016;101:157-168.

[15] Wang JF, Wang J, Wang H. Seismic behavior of blind bolted CFST frames with semi-rigid connections. Structures 2017;9:91-104.

[16] Loh HY, Uy B, Bradford MA. The effects of partial shear connection in composite flush end plate joints Part I-experimental study. Journal of Constructional Steel Research 2006;62:378-390.

[17] Mirza O, Uy B. Behaviour of composite beam–column flush end-plate connections subjected to low-probability, high-consequence loading. Engineering Structures 2011;33:647-662.

[18] Ataei A, Bradford MA, Valipour HR. Experimental study of flush end plate beam-to-CFST column composite joints with deconstructable bolted shear connectors. Engineering Structures 2015;99:616-630.

[19] Ataei A, Bradford MA, Valipour HR, Liu X. Experimental study of sustainable high strength steel flush end plate beam-to-column composite joints with deconstructable bolted shear connectors. Engineering Structures 2016;123:124-140.

[20] Ataei A, Bradford MA, Liu X. Experimental study of flush end plate beam-to-column composite joints with precast slabs and deconstructable bolted shear connectors. Structures 2016;7:43-58.

[21] Agheshlui H, Goldsworthy H, Gad E, Mirza O, Sr. Anchored blind bolted composite connection to a concrete filled steel tubular column. Steel and Composite Structures 2017;23:115-130.

[22] Song TY, Tao Z, Razzazzadeh A, Han LH, Zhou K. Fire performance of blind bolted composite beam to column joints. Journal of Constructional Steel Research

2017;132:29-42.

[23] Wang JF, Zhang H. Seismic performance assessment of blind bolted steel-concrete composite joints based on pseudo-dynamic testing. Engineering Structures 2017;131:192-206.

[24] Thai HT, Uy B, Yamesri, Aslani F. Behaviour of bolted endplate composite joints to square and circular CFST columns. Journal of Constructional Steel Research 2017;131:68-82.

[25] Tao Z, Hassan MK, Song T-Y, Han L-H. Experimental study on blind bolted connections to concrete-filled stainless steel columns. Journal of Constructional Steel Research 2017;128:825-838.

[26] Thai HT, Uy B. Rotational stiffness and moment resistance of bolted endplate joints with hollow or CFST columns. Journal of Constructional Steel Research 2016;126:139-152.

[27] Wang JF, Spencer Jr BF. Experimental and analytical behavior of blind bolted moment connections. Journal of Constructional Steel Research 2013;82:33-47.

[28] Wang JF, Zhang N, Guo S. Experimental and numerical analysis of blind bolted moment joints to CFTST columns. Thin-Walled Structures 2016;109:185-201.

[29] Wang JF, Zhang N. Performance of circular CFST column to steel beam joints with blind bolts. Journal of Constructional Steel Research 2017;130:36-52.

[30] Kataoka MN, de Cresce El Debs ALH. Beam–column composite connections under cyclic loading: an experimental study. Materials and Structures 2015;48:929-946.

[31] Kataoka MN, El Debs ALHC. Parametric study of composite beam-column connections using 3D finite element modelling. Journal of Constructional Steel

Research 2014;102:136-149.

[32] Ataei A, Bradford M, Valipour H. Moment-rotation model for blind-bolted flush end-plate connections in composite frame structures. Journal of Structural Engineering 2014;141:04014211.

[33] Thai HT, Uy B. Finite element modelling of blind bolted composite joints. Journal of Constructional Steel Research 2015;112:339-353.

[34] Ataei A, Bradford MA, Valipour HR. Finite element analysis of HSS semi-rigid composite joints with precast concrete slabs and demountable bolted shear connectors. Finite Elements in Analysis and Design 2016;122:16-38.

[35] Ataei A, Bradford MA, Liu X. Computational modelling of the moment-rotation relationship for deconstructable flush end plate beam-to-column composite joints. Journal of Constructional Steel Research 2017;129:75-92.

[36] Ataei A, Bradford MA. Numerical study of deconstructable flush end plate composite joints to concrete-filled steel tubular columns. Structures 2016;8:130-143.

[37] Yu H, Burgess IW, Davison JB, Plank RJ. Numerical simulation of bolted steel connections in fire using explicit dynamic analysis. Journal of Constructional Steel Research 2008;64:515-525.

[38] ABAQUS. User's Manual, Version 6.13: Dassault Systemes Corp., Providence, RI, USA; 2013.

[39] Egan B, McCarthy CT, McCarthy MA, Gray PJ, Frizzell RM. Modelling a single-bolt countersunk composite joint using implicit and explicit finite element analysis. Computational Materials Science 2012;64:203-208.

Table Captions

Table 1. Material properties of structural steels

Table 2. CPU times on 3.6 GHz Core i7 with 32 GB RAM

Table 3. Applied load and corresponding displacement at critical points

Table 1. Material properties of structural steels

Component	Yield stress (MPa)	Ultimate stress (MPa)	Elongation at fracture (%)
Column	351	514	16
Beam web	393	535	19
Beam flange	351	514	16
Rebar	596	683	15
Profiled sheeting	549	554	6
Shear connector	447	532	24
M20 Hollo-bolt	984	1040	16

Table 2. CPU times on 3.6 GHz Core i7 with 32 GB RAM

Hollo-bolt mesh	Number of element for one bolt	DOF of whole model	CPU time (h)
Mesh 1 (see Fig. 13a)	208	41,792	0.32
Mesh 2 (see Fig. 13b)	896	73,817	1.13
Mesh 3 (see Fig. 13c)	3,552	159,650	4.45

Table 3. Applied load and corresponding displacement at critical points

Critical point	Applied load (kN)	Displacement (mm)	Note
1	21.35	0.46	Initial crack in concrete slab
2	128.30	4.32	Yielding in bottom flange
3	139.71	4.92	Yielding in headed stud
4	223.96	11.22	Yielding in endplate
5	266.21	16.45	Yielding in steel column
6	278.35	18.77	Yielding in reinforcing bars
7	291.86	23.75	Yielding in profiled sheeting
8	300.81	29.07	Full crack in concrete slab
9	308.00	41.62	Local buckling in the bottom flange and web of steel beam

Figure Captions

Fig. 1. Typical blind bolted endplate composite beam-to-CFST column connection

Fig. 2. Configuration details of specimen CJ1 tested by Loh et al. [16]

Fig. 3. FE model of a half of the specimen

Fig. 4. FE mesh of a half of the specimen

Fig. 5. Effect of *smooth step*

Fig. 6. Smooth step and linear step amplitudes

Fig. 7. Effect of mass scaling

Fig. 8. Effect of loading rates
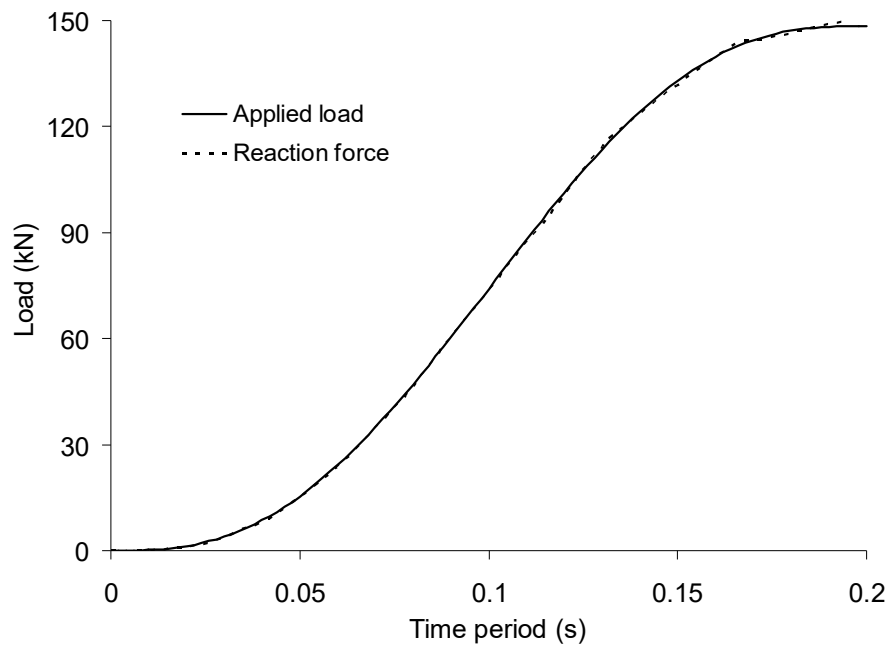
Fig. 9. Energy results of the whole model at different loading rates

Fig. 10. Effect of loading rates on KE-to-IE ratio

Fig. 11. Comparison of applied loads and reaction forces at different loading rates

Fig. 12. Geometry of Hollo-bolt
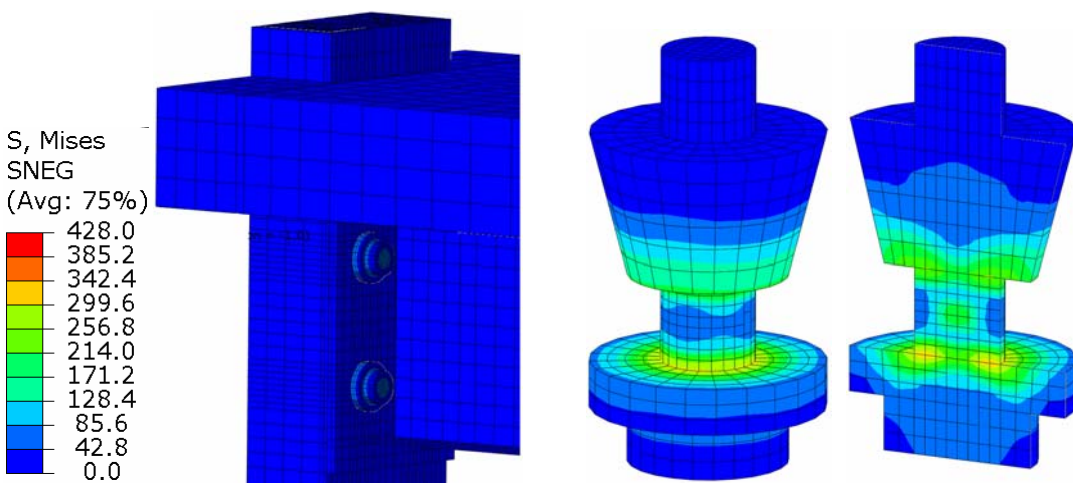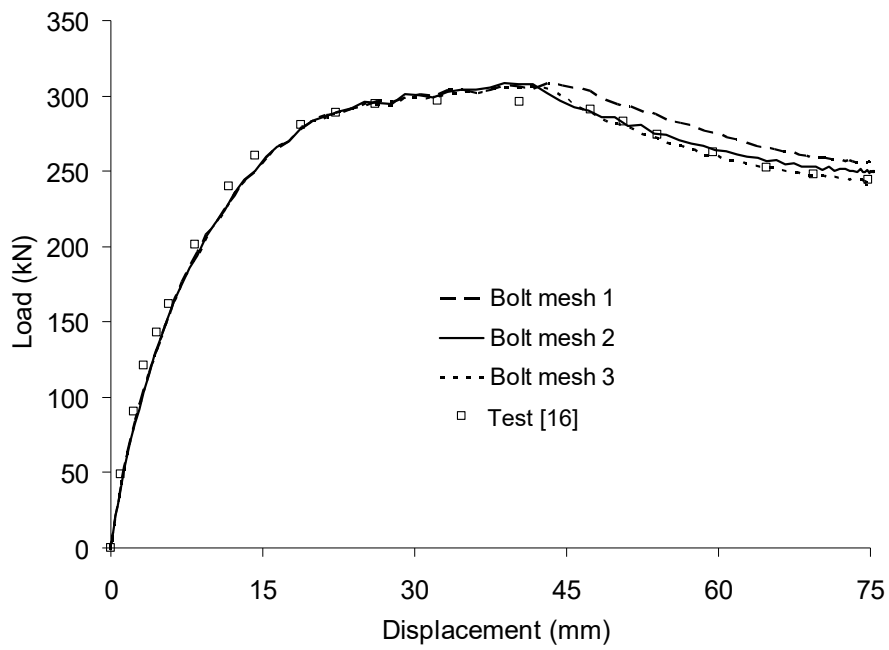
Fig. 13. Mesh for Hollo-bolt
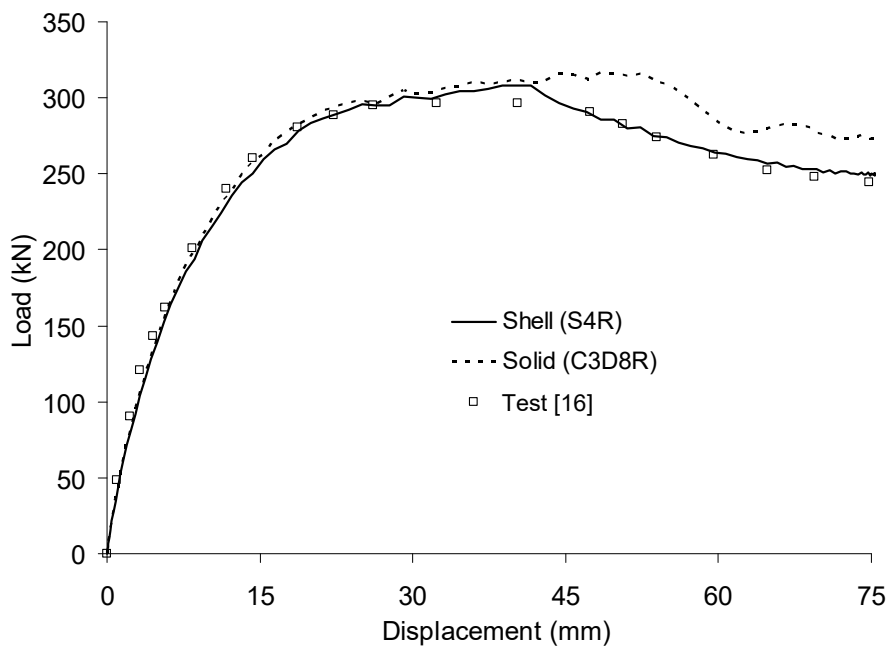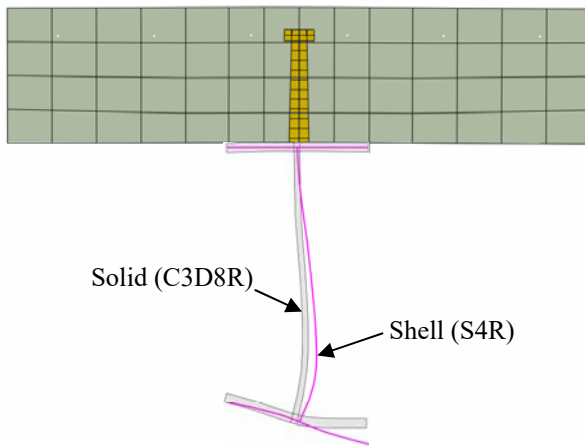
Fig. 14. Von Mises stress due to bolt pretension

Fig. 15. Effect of bolt mesh sizes

Fig. 16. Effect of element types used to model the steel beam

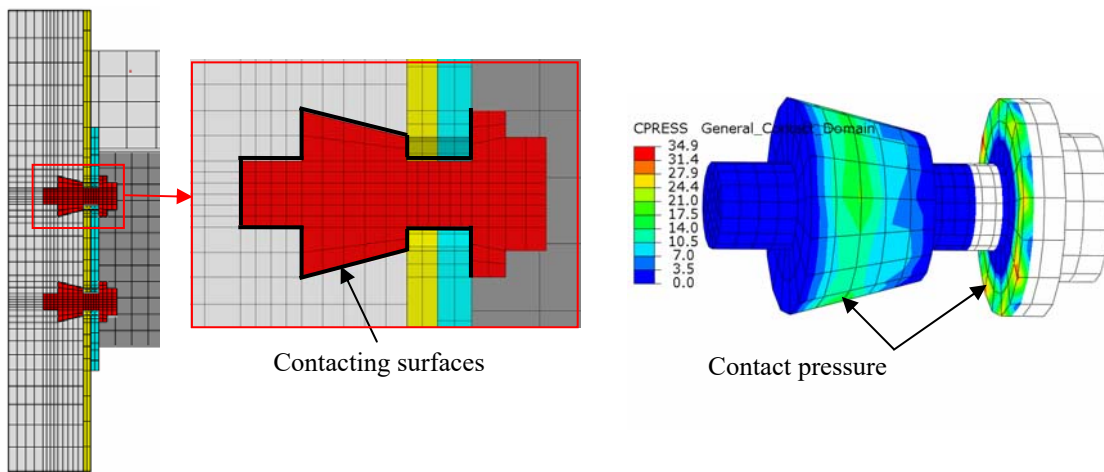Fig. 17. Effect of element type in capturing the local buckling of the steel beam

Fig. 18. Contacting surfaces and contact pressure in the bolt due to bolt pretension

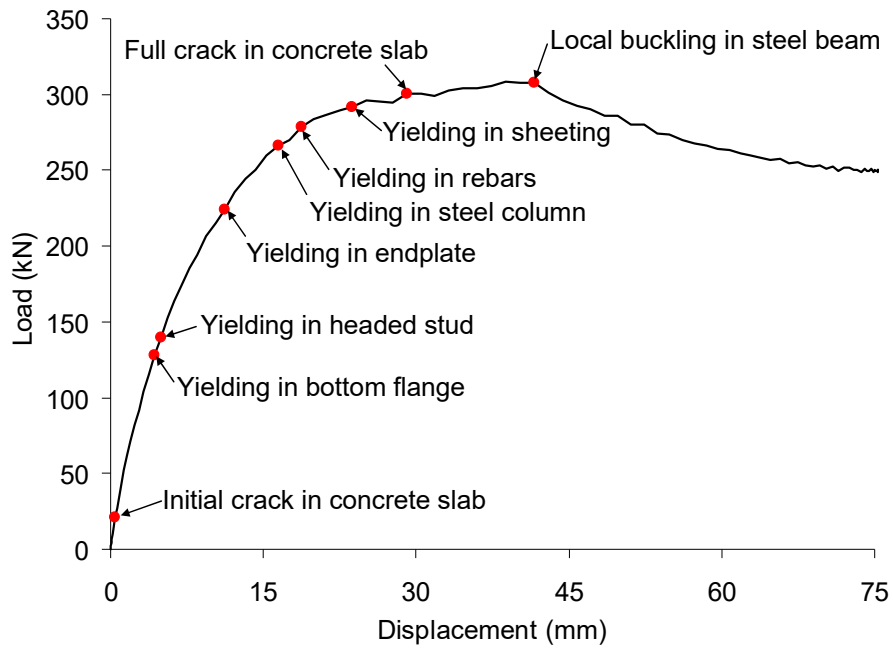Fig. 19. Load-displacement responses of the connection with critical points

Fig. 20. Von Mises stress distribution in each component at the ultimate load

Fig. 21. Tensile damage parameter in concrete slab

Fig. 22. Load-crack width response

Fig. 1. Typical blind bolted endplate composite beam-to-CFST column connection
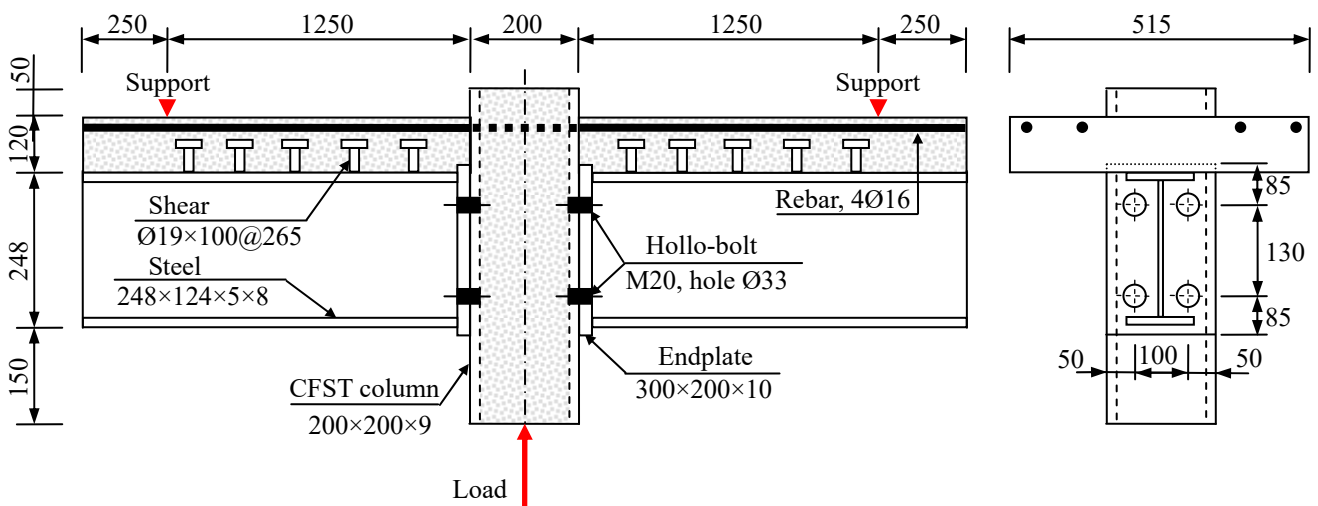
Fig. 2. Configuration details of specimen CJ1 tested by Loh et al. [16]
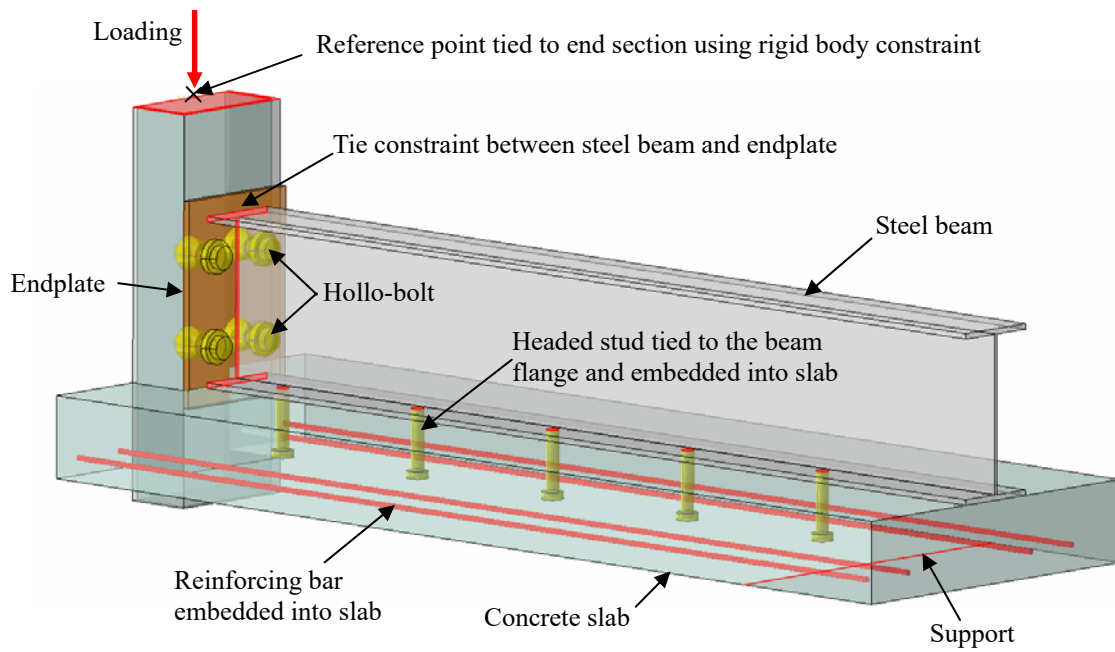
Fig. 3. FE model of a half of the specimen
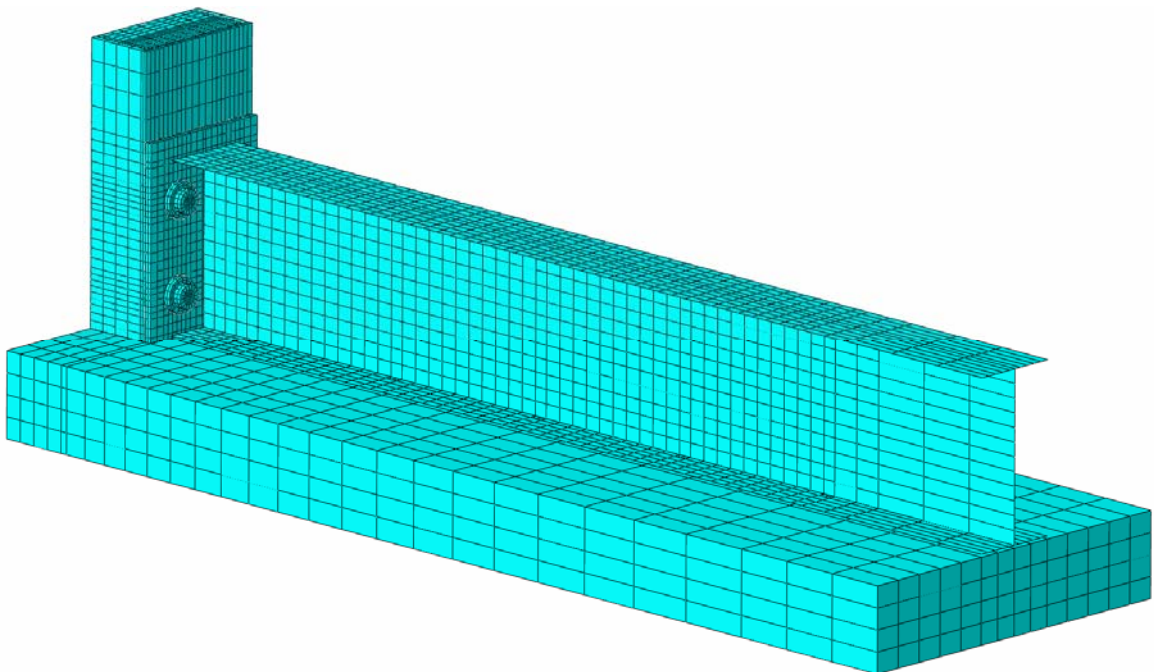
Fig. 4. FE mesh of a half of the specimen
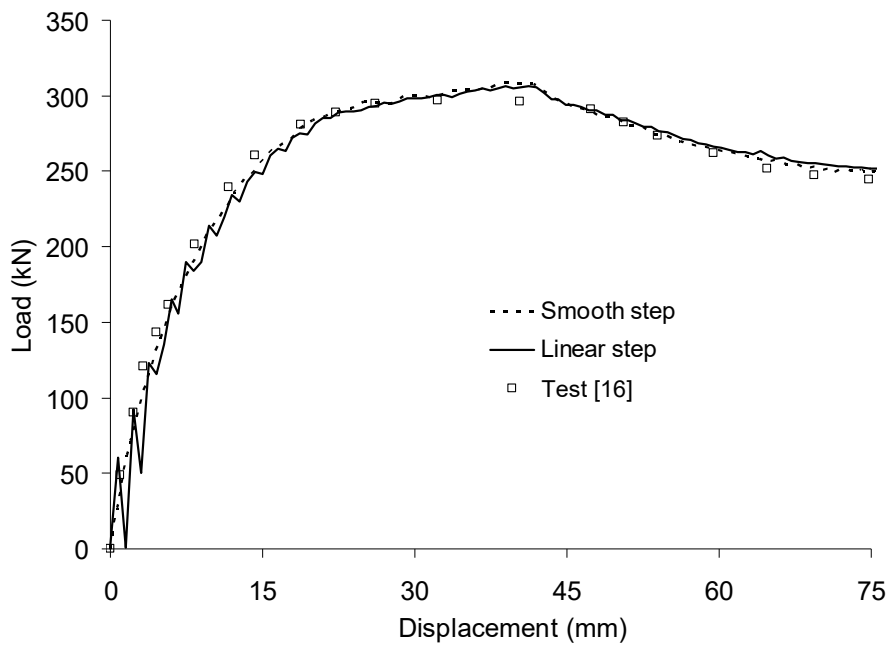
Fig. 5. Effect of *smooth step*
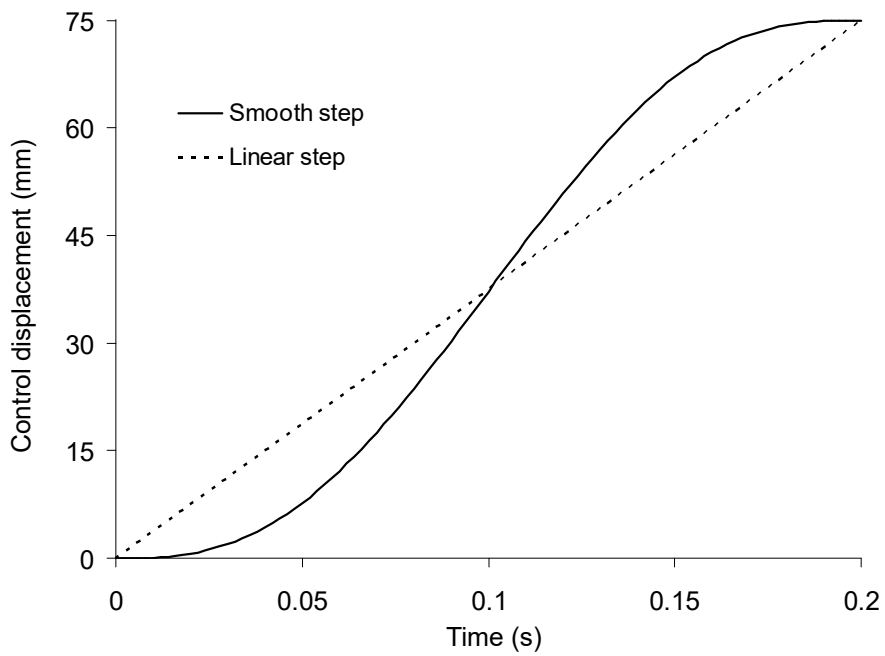
Fig. 6. Smooth step and linear step amplitudes
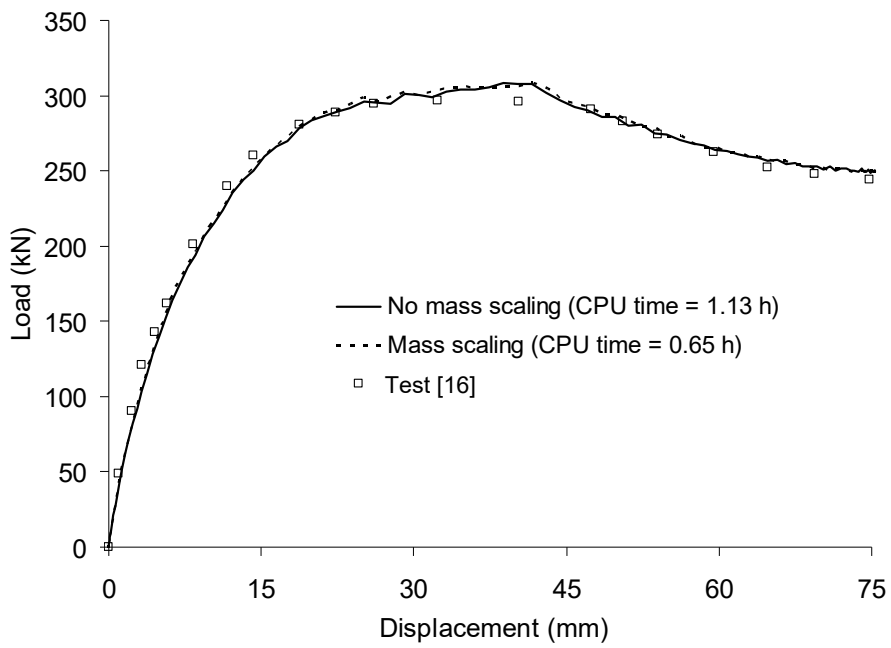
Fig. 7. Effect of mass scaling
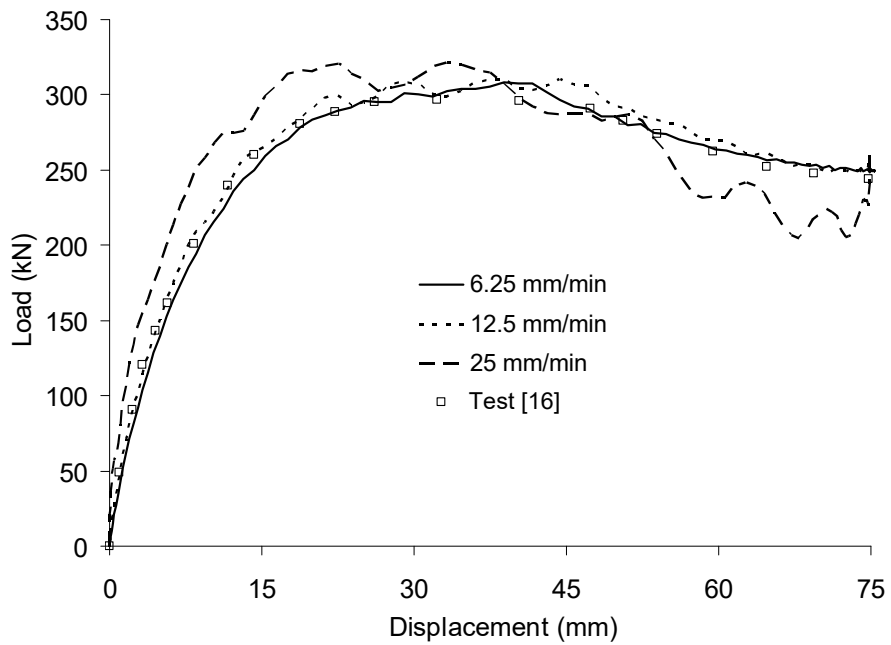
Fig. 8. Effect of loading rates
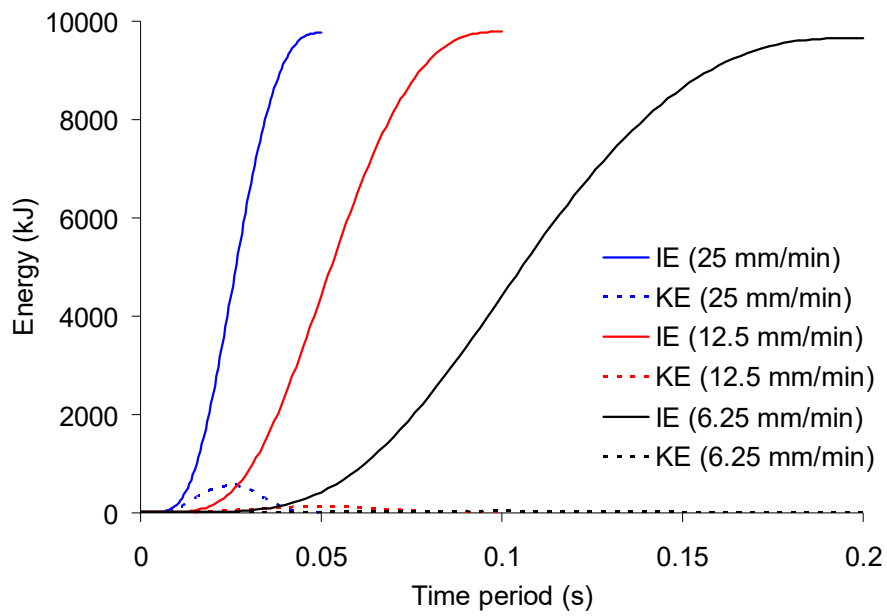
Fig. 9. Energy results of the whole model at different loading rates
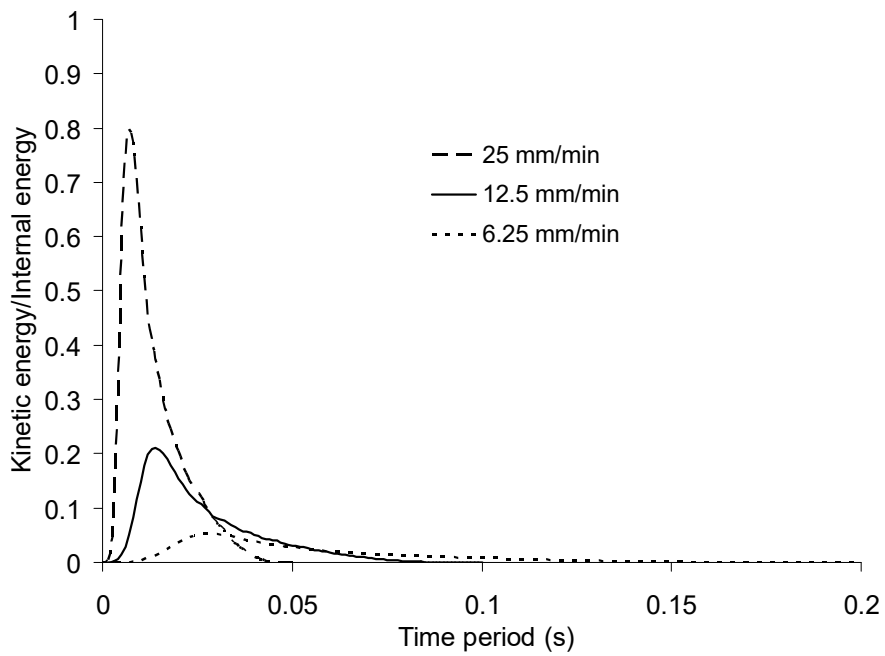
Fig. 10. Effect of loading rates on KE-to-IE ratio
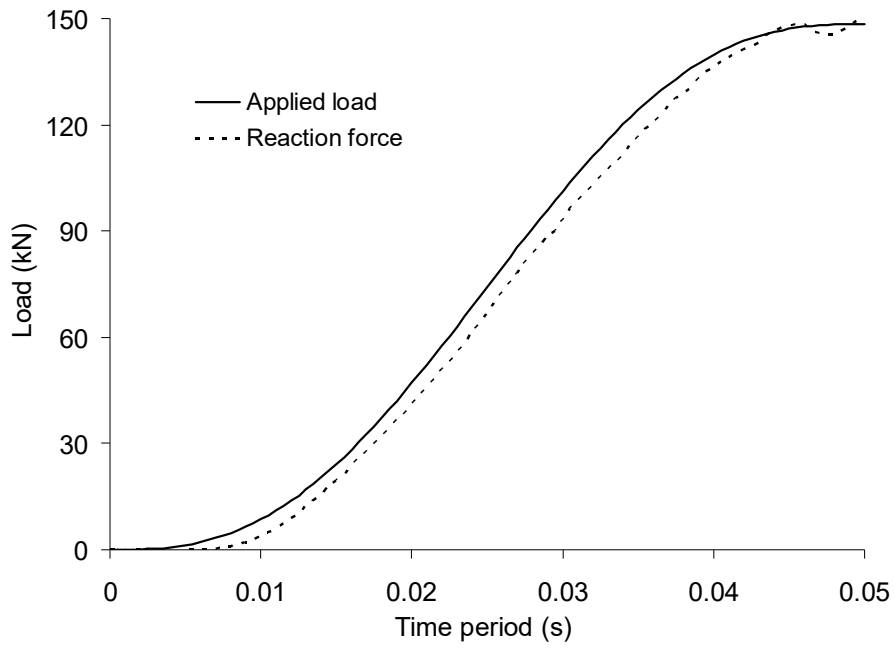
(a) Loading rate of 25 mm/min
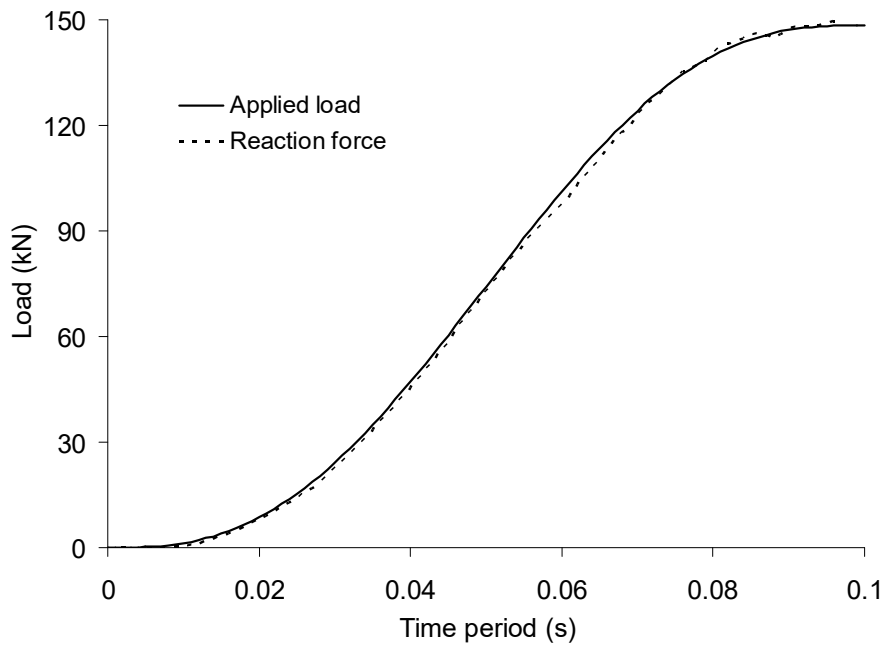
(b) Loading rate of 12.5 mm/min

28

(c) Loading rate of 6.25 mm/min

Fig. 11. Comparison of applied loads and reaction forces at different loading rates
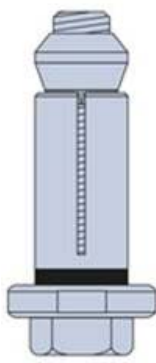
(a) Before tightening   (b) After tightening   (c) Simplified model
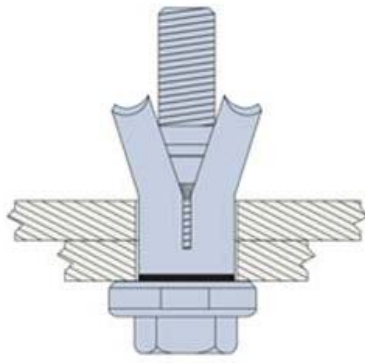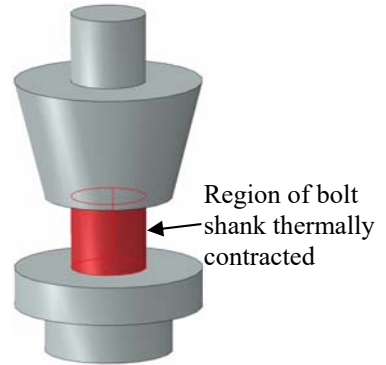
Fig. 12. Geometry of Hollo-bolt
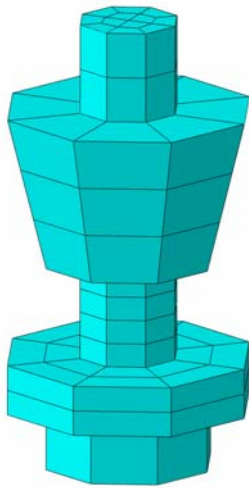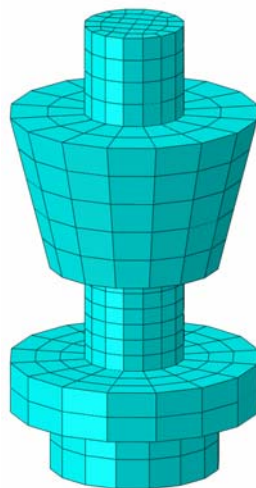
(a) Mesh 1: 8×2   (b) Mesh 2: 16×3   (c) Mesh 3: 24×4
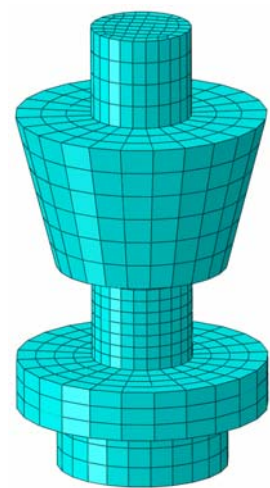
Fig. 13. Mesh for Hollo-bolt
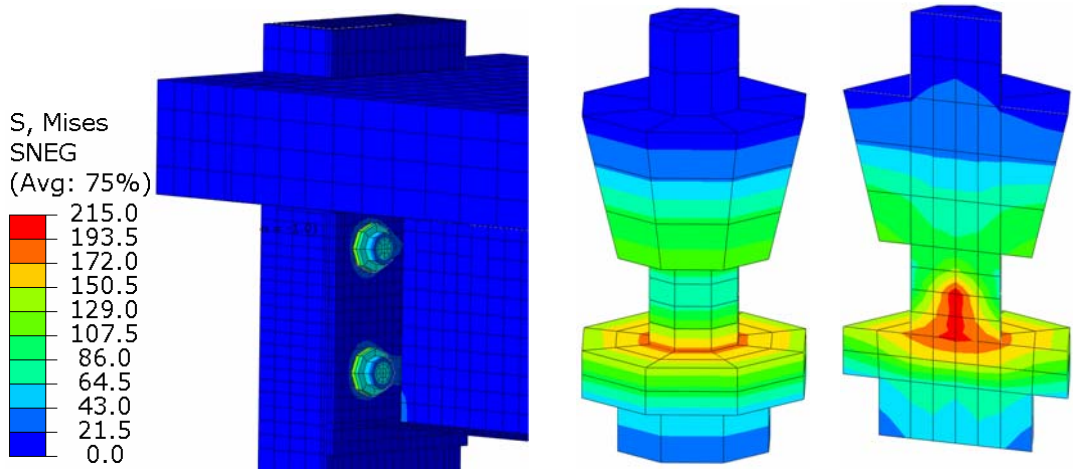
(a) Mesh 1
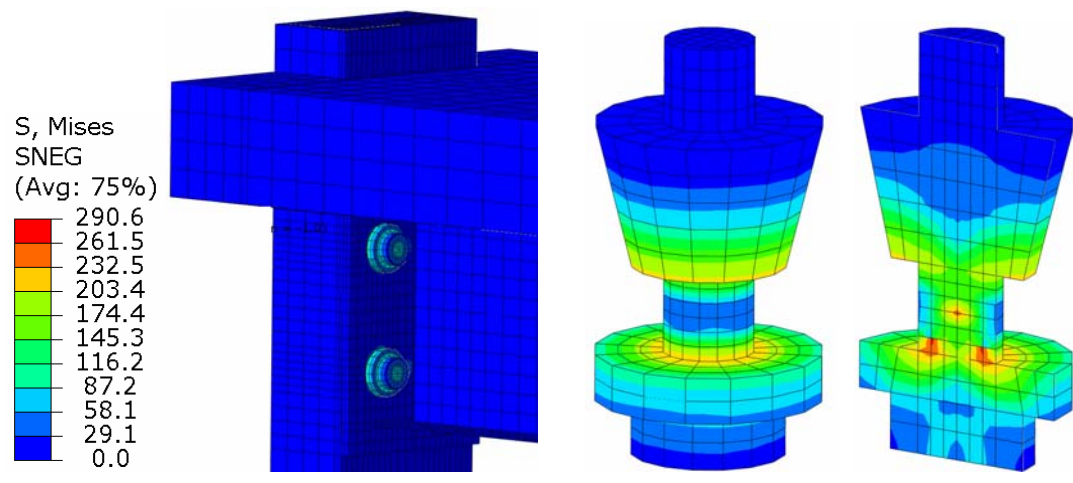
(b) Mesh 2

(c) Mesh 3

Fig. 14. Von Mises stress due to bolt pretension

Fig. 15. Effect of bolt mesh sizes

Fig. 16. Effect of element types used to model the steel beam

(a) FE simulation   (b) Test [16]

Fig. 17. Effect of element type in capturing the local buckling of the steel beam

Fig. 18. Contacting surfaces and contact pressure in the bolt due to bolt pretension

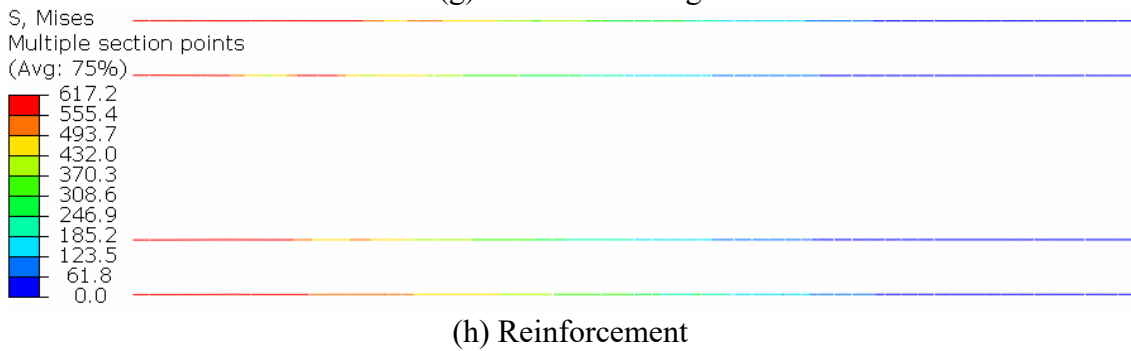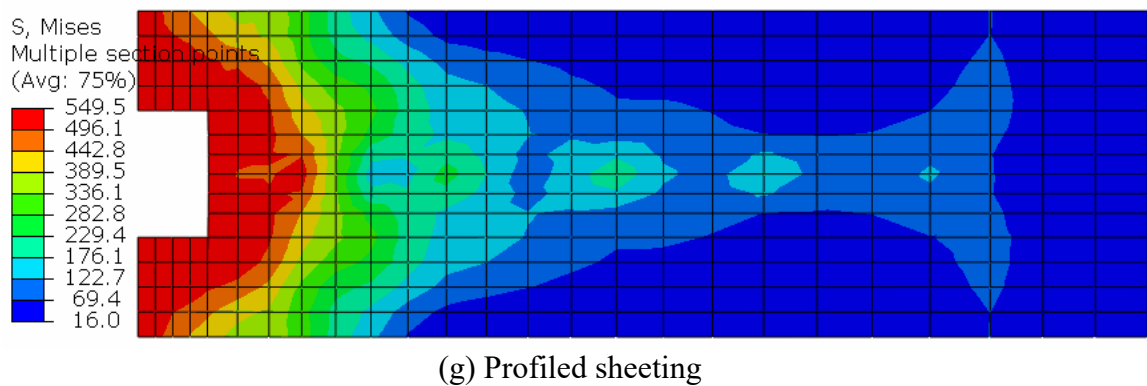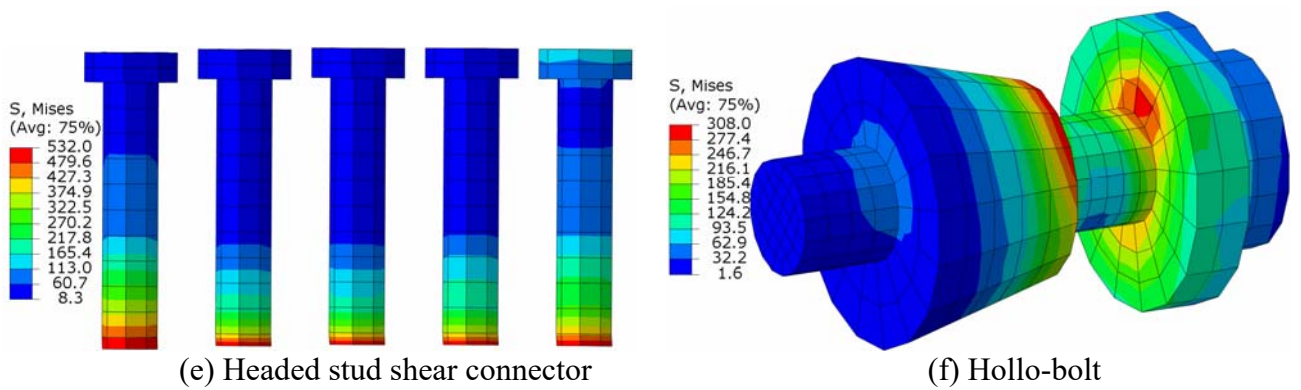Fig. 19. Load-displacement responses of the connection with critical points

(a) Infilled concrete

(b) steel column

(c) Endplate

(d) Steel beam

(e) Headed stud shear connector

(f) Hollo-bolt

(g) Profiled sheeting

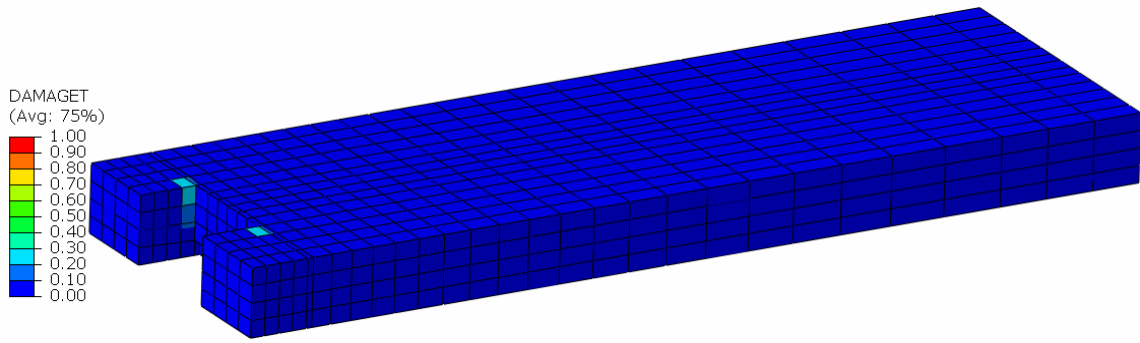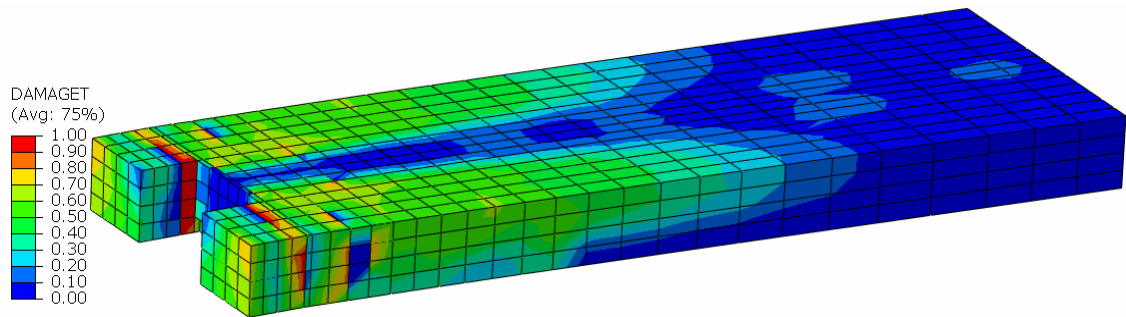(h) Reinforcement
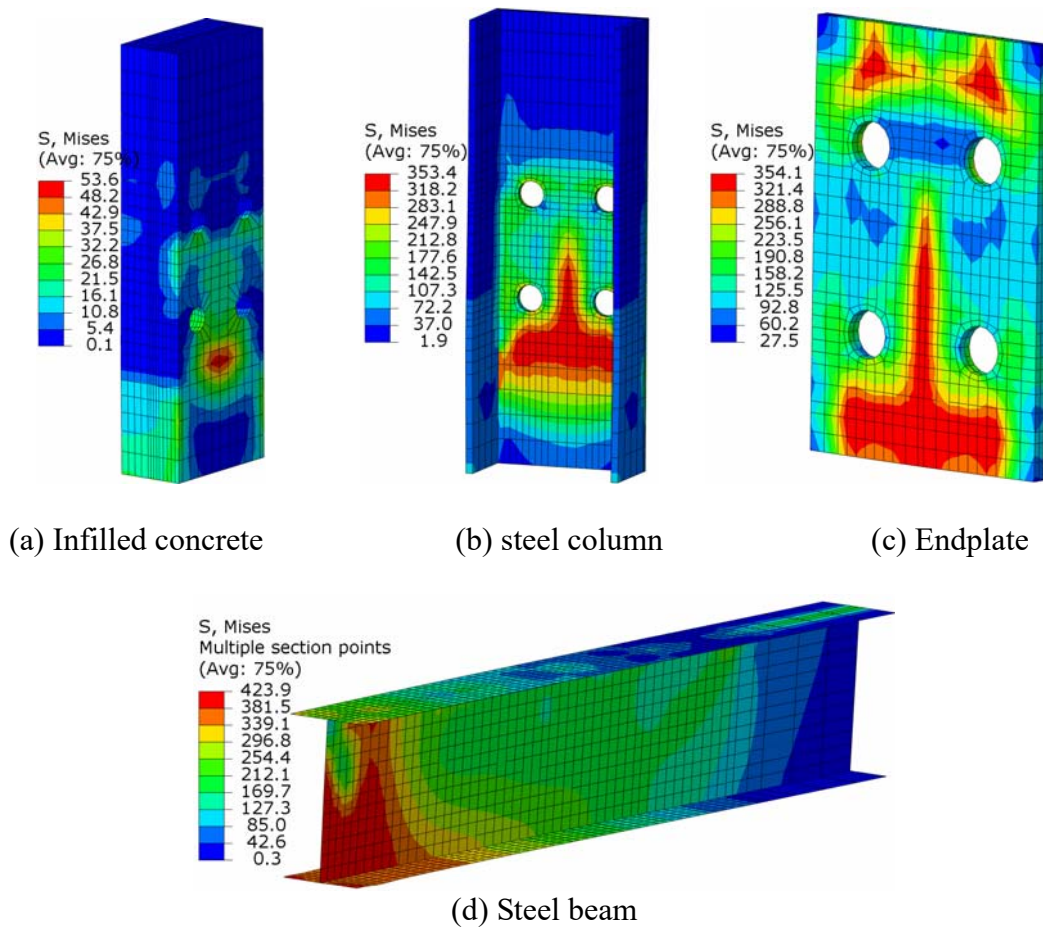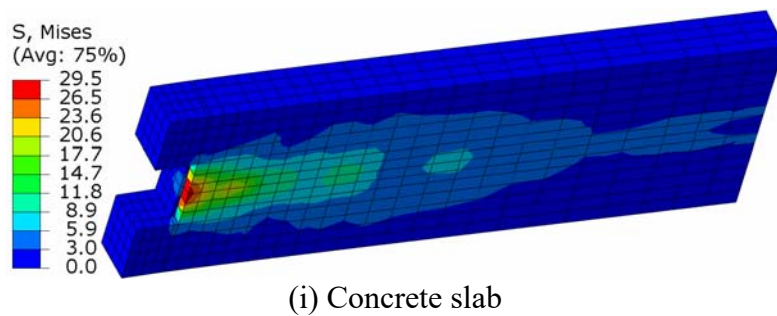
(i) Concrete slab

Fig. 20. Von Mises stress distribution in each component at the ultimate load

(a) Initial crack
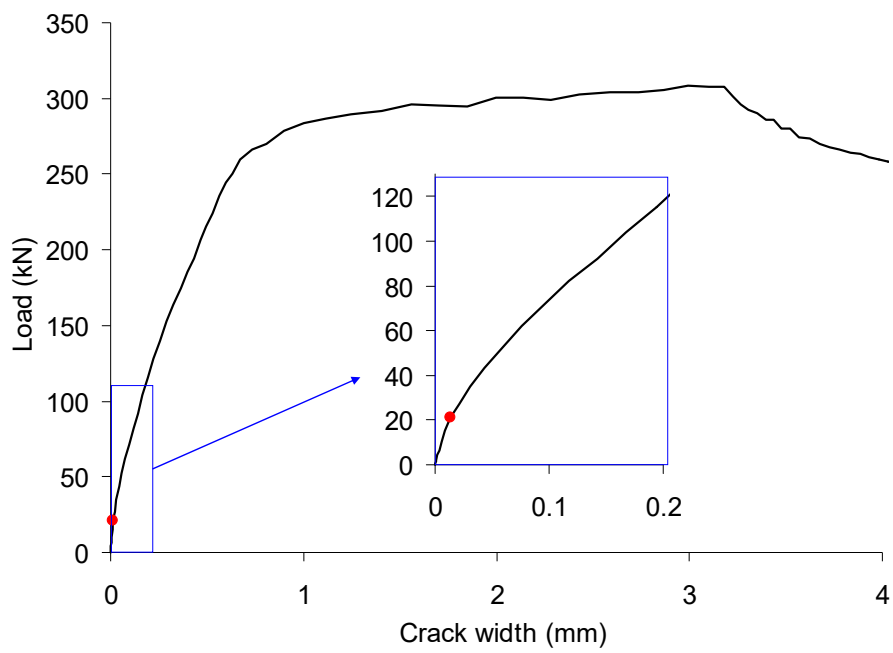

(b) Crack at the ultimate load

Fig. 21. Tensile damage parameter in concrete slab

Fig. 22. Load-crack width response